



Motional narrowing of molecular vibrations strongly coupled to surface lattice resonancesFrancesco Verdelli *Dutch Institute for Fundamental Energy Research DIFFER, Eindhoven 5600HH, The Netherlands*

Andrea Baldi

*Vrije Universiteit Amsterdam, Amsterdam 1081HV, The Netherlands*Jaime Gómez Rivas **Department of Applied Physics and Science Education, Hendrik Casimir Institute, Institute for Complex Molecular Systems, Eindhoven University of Technology, Eindhoven 5600MB, The Netherlands* (Received 8 November 2023; revised 28 March 2024; accepted 24 April 2024; published 7 May 2024)

We report on strong coupling between light in open cavities formed by arrays of gold microparticles and the carbonyl molecular vibration in poly(methyl methacrylate). These arrays sustain surface lattice resonances (SLRs), which are optical modes generated by the enhanced radiative coupling of the localized resonances in single scatterers by the diffraction in the array. Using the high-coherence beam of a free-electron laser, we measure the vibrational strong coupling and find a Rabi splitting into an upper and lower vibropolariton band. We observe the narrowing of the lower polariton band when the SLR is resonant with the molecular vibration. This behavior of the lower polariton linewidth can be modeled taking into account motional narrowing due to the spatial averaging of delocalized molecular vibrations in the strong coupling regime. The presence of motional narrowing in vibropolaritons in plasmonic arrays gives insight into the strong coupling of molecular vibrations, and introduces a different platform to investigate polaritonic chemistry, where reactions are not governed by individual molecules but by collective coupled vibrations.

DOI: [10.1103/PhysRevB.109.174305](https://doi.org/10.1103/PhysRevB.109.174305)**I. INTRODUCTION**

The spectral linewidth defined by a set of resonators distributed in a medium is usually influenced by the broadening caused by fluctuations in this medium. Variations of the resonance frequency from point to point lead to an apparent broadening of the linewidth known as inhomogeneous broadening. When a resonator moves within this medium, the linewidth undergoes a narrowing effect due to spatial averaging processes [1], which enhances the coherent response of the resonator while mitigating the impact of random or disorder-induced variations on the linewidth, resulting in a distinct and well-defined resonance. Known as motional narrowing, this reduction in linewidth is a prevalent occurrence observed in various systems. For example, it is known in molecular systems where vibrational modes of individual molecules are influenced by the neighboring ones. If these neighboring molecules rearrange themselves fast enough, the vibrational resonance will occur at an averaged frequency with a narrower linewidth [2–4]. Motional narrowing has been also shown experimentally and theoretically with exciton polaritons in semiconductor Fabry-Perot microcavities [5–8], in semiconductor quantum wells [9,10], quantum dots [11–13], and in atomically thin semiconductors under strong light-matter coupling [14]. Strong light-matter coupling corresponds to the

regime where the energy exchange rate between matter and the field in an optical cavity is faster than the decoherence or loss rates of the bare matter excitation and the light in the cavity [15–18]. Two new hybrid states are formed, the upper (UP) and lower (LP) polaritons in this regime, and they are split in energy, as shown in Fig. 1(a). This energy difference is known as the vacuum Rabi splitting and is given by [19]

$$\hbar\Omega = 2\sqrt{N}\mathbf{E} \cdot \mathbf{d} = 2\sqrt{N}\sqrt{\frac{\hbar\omega_0}{2\varepsilon_0V}}d \cos\theta, \quad (1)$$

where Ω is the Rabi frequency, \mathbf{E} is the vacuum electric field of the cavity mode, \mathbf{d} is the transition dipole moment of the molecules, N is the number of molecules in the cavity, ω_0 is the resonant frequency of the cavity, and V is the mode volume. Since motional narrowing is very sensitive to the degree of delocalization of the excitations, vibrational strong coupling allows one to tune such degree and it is, therefore, an ideal platform to search for or control motional narrowing.

In this manuscript, we demonstrate the presence of motional narrowing in vibropolaritons, originating from the strong coupling between the C=O bond of poly(methyl methacrylate) (PMMA) and collective resonances in arrays of gold microparticles. These arrays of metallic particles sustain surface lattice resonances (SLRs), which are modes that result from the enhanced radiative coupling of the localized plasmonic resonances in individual particles by diffraction orders in the plane of the array [Rayleigh anomalies (RAs)]. SLRs

*j.gomez.rivas@tue.nl

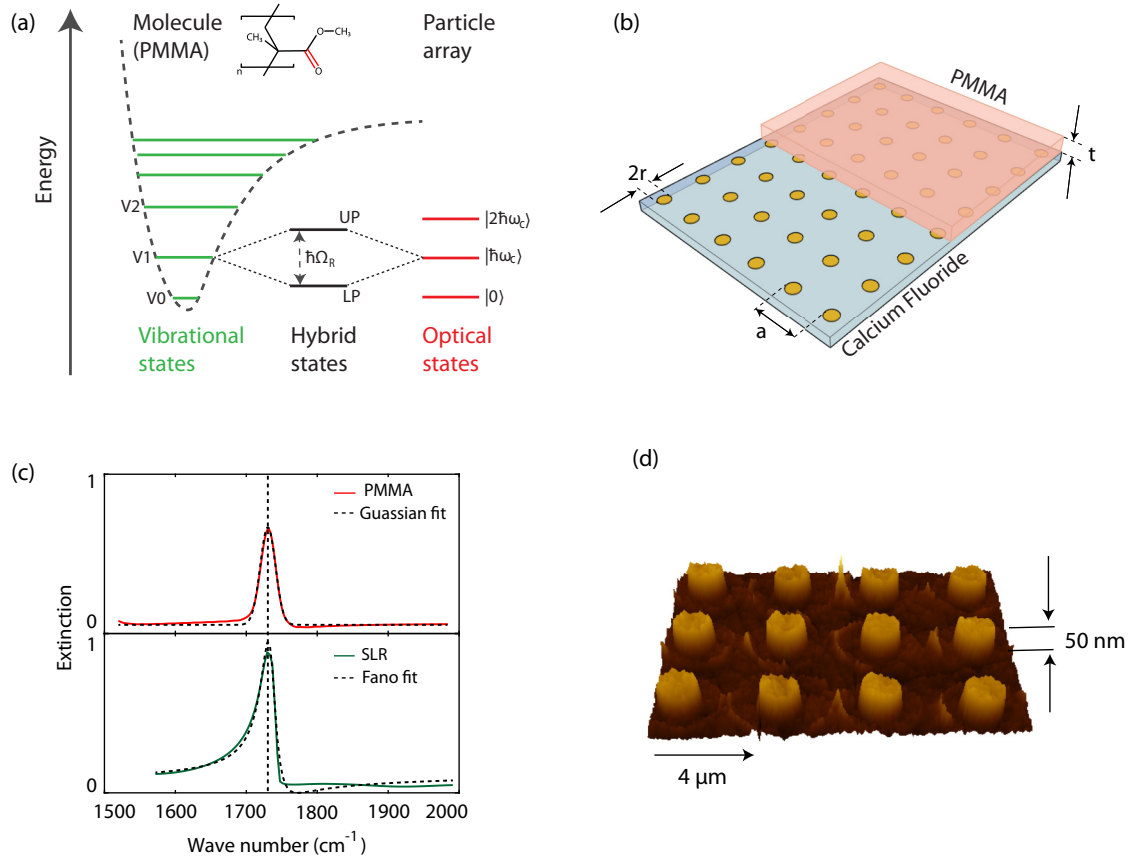


FIG. 1. (a) Jablonsky diagram of the strongly coupled system. The vibrational states of the PMMA molecules are represented in green. The optical modes of the cavity are represented in red. The hybrid vibrational/optical states are represented in black. The molecular structure of PMMA is shown in the inset, with the C=O bond highlighted in red. (b) Schematic representation of the system under investigation. r , a , and t are the parameters optimized with simulations. (c) Simulated extinction of the PMMA layer with a thickness of 700 nm and the SLR of the bare particle array (700 nm radius, 50 nm height, and 4 μm period). The dotted lines are the Gaussian fit for the molecular peak and the Fano fit for the SLR. The vertical dotted line indicates the spectral peak position of both resonances. (d) 3D atomic-force-microscope image of the particle array with 4 μm period.

are thus the result of the hybridization of localized resonances with diffraction orders [20]. The characteristics of SLRs are a consequence of their hybrid nature [21–24]: they show high field enhancements from their plasmonic character, and a delocalization of the electric field in the surrounding medium from their photonic character [25,26]. The combination of these characteristics makes SLRs an attractive instrument to investigate light matter, and they could be used to modify the kinetics of chemical reactions under the strong coupling regime [19,27,28]. SLRs have already shown their potential in applications such as sensing [29–33], spectroscopy [34–36], and electrochemistry [37,38]. Recently, SLRs have been shown to strongly couple with molecular vibrations [39,40], making them a possible alternative to Fabry-Perot cavities as a method to investigate strong light-matter interactions. Furthermore, when comparing to the closed system of Fabry-Perot cavities, these arrays of plasmonic particles provide accessibility to their surface. As a result, they can be easily coupled with external radiation, allowing for a more convenient characterization of the motional narrowing of vibropolaritons.

Here, we use a free-electron laser (FEL) light source for the investigation of the effects of motional narrowing on the

polaritons linewidth. Compared to conventional methods of IR spectroscopy such as Fourier transform infrared spectroscopy (FTIR), a FEL is a high-intensity and coherent source that experimentally minimizes the broadening of the SLR. Using this FEL, we characterize the PMMA-SLRs coupled system performing direct transmission measurements and determining the Rabi splitting. Here we investigate the vibrational strong coupling using a FEL. We model the frequency and the linewidth of the polaritons with a coupled oscillator model to retrieve the mixing or Hopfield coefficients of the system. Finally, we show that the narrowing of the lower polariton linewidth as a function of the Hopfield coefficient can be explained by taking into account motional narrowing.

II. SAMPLE DESCRIPTION

The demonstration of motional narrowing of vibropolaritons is performed using a uniform array of gold microdisks embedded in a layer of PMMA as the optical cavity. The optimal geometry of the open cavity is found when the SLR of the gold microparticle array perfectly overlaps with the resonance of the C=O stretching in the extinction spectrum. First, we simulate a system with periodic boundary conditions. The

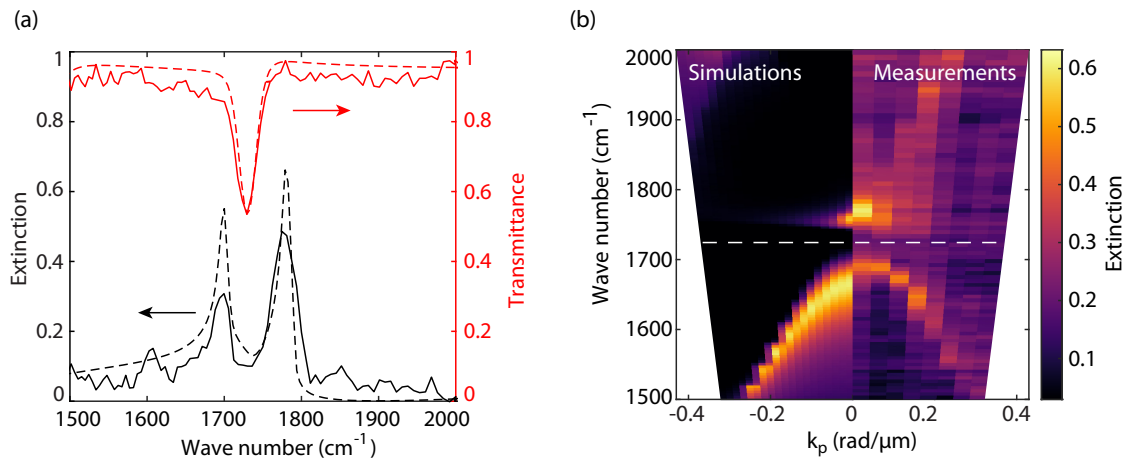


FIG. 2. Analysis of the C=O-SLR coupling. (a) Extinction measurement (solid black) and simulations (dashed black) of the coupled system. Transmittance measurements (solid red) and simulations (dashed red) of the bare PMMA film. (b) Extinction map of the coupled system as a function of the incident wave vector parallel to the surface of the array. The simulations are shown on the left side of the panel and the measurements are shown on the right side.

elements of the system are a semi-infinite substrate of CaF₂, a gold microparticle, and a layer on top as the upperstrate. The complex permittivity of CaF₂ and gold is taken from Refs. [41,42]. The complex refractive index ($\tilde{n} = n + i\kappa$) of PMMA in the mid-IR can be approximated as a constant real component $n = 1.44$ and a nonzero extinction coefficient κ leading to a dispersive peak at 1732 cm^{-1} , due to the stretching of the C=O double bond. To simulate the optical response of the array without any interference from its coupling to the carbonyl stretching of PMMA, we first define the top layer in the simulations as a dielectric material with constant refractive index of $n = 1.44$ and no absorption. The optical response of the array is investigated by using finite-difference time-domain (FDTD) simulations and sweeping over different values of radius of the particles, r , period of the array, a , and thickness of the molecular layer, t . A schematic of the investigated system with the FDTD simulations is shown in Fig. 1(b). From the simulations, we obtain the geometrical parameters that ensure a good overlap between the C=O bond of PMMA and the array's SLR in extinction (E), defined as $E = 1 - T$, where T is the transmittance, as can be seen in Fig. 1(c). These parameters are microparticle radius of 700 nm and height of 50 nm, and PMMA layer with thickness of 700 nm. The period of the array is $4 \mu\text{m}$. The total simulated electric field associated to the SLR is shown in the Supplemental Material (SM), Sec. S1 [43].

The tuned array and a series of periodic arrays with SLRs covering a range of energies around the C=O resonance are fabricated on CaF₂ substrates using UV optical lithography (see SM, Sec. S2) [43]. A three-dimensional (3D) atomic-force-microscope image of an array of particles used to couple with PMMA is shown in Fig. 1(d).

III. RESULTS AND DISCUSSION

A. Vibrational strong coupling measured with a free-electron laser

To study the PMMA and microparticle array system, we begin by simulating it with a top layer composed of a material

with wavelength-dependent permittivity, as described in [44]. Then, we experimentally investigate the coupled system by spin coating a 700-nm-thick PMMA layer onto the array (for further details, refer to Sec. S2 in the SM) [43]. We characterize the coupled system by measuring the IR transmission with a FEL, situated at the Free Electron Laser for Infrared Experiments (FELIX) Laboratory at the High Field Magnet Laboratory (HFML). The FEL beam has an elliptical shape with long and short axis of 3 mm and 2 mm, respectively. The signal is detected with a Spiricon Pyrocam beam profiler. Typical measured spectra obtained by scanning the FEL wavelength are shown in Fig. 2(a), where a comparison of simulated (dotted curve) and measured (solid curve) transmittance and extinction of the C=O molecular stretching and of the coupled system, respectively, are shown. Both simulated and measured spectra are at normal incidence. The upper and lower polaritons are clearly visible in the extinction spectra [black curves in Fig. 2(a)]. The frequencies of the measured polaritons are in good agreement with the simulated ones. In particular, the lower polariton is observed at 1700 cm^{-1} and the upper polariton at 1776 cm^{-1} . We retrieve, thus, a Rabi splitting of 76 cm^{-1} . Previous measurements performed on the same system with a Fourier transform infrared spectrometer (FTIR) show an identical Rabi splitting [40]. The noise in the measurements is caused by the instability of the FEL. The measured PMMA peak is slightly broader than the simulation. This mismatch is most likely caused by the spectral tunability of the FEL, which is limited to $\approx 6 \text{ cm}^{-1}$ in our measurements. Another important difference between the simulations and the measurements is the intensity of the polariton peaks in the extinction spectrum. This difference is most likely caused by losses due to fabrication imperfections. These measurements are repeated for arrays with period ranging from $3.7 \mu\text{m}$ to $4.2 \mu\text{m}$ (SM, Sec. S3) [43]. In Fig. 2(b), the simulated (left panel) and measured (right panel) extinction spectra for the array with $4 \mu\text{m}$ period are plotted as function of the incident angle θ of the FEL beam. This dependence is studied for s -polarized incident light by detecting the zeroth-order transmission at different angles and it is plotted as function of wave

vector parallel to the surface of the array, $k_p = (2\pi/\lambda) \sin \theta$. The dispersion of the upper and lower polaritons is clearly visible above and below the C=O stretching frequency [dotted white line in Fig. 2(b)]. We measure the Rabi splitting at the wave vector where the separation between the two extinction bands of the polaritons is the smallest, which corresponds to normal incidence ($\hbar\Omega = 76 \text{ cm}^{-1}$), thus confirming that the molecular vibration is coupled with the SLR of the array.

In addition, a slight but consistent blueshift of the experiments compared to the simulations is present in Fig. 2(b), which we attribute to a small difference between the actual refractive index and the one used in the FDTD model ($n = 1.44$). To properly determine that the system is in the strong coupling regime and to retrieve the molecular and photonic composition of the vibropolaritons, we use a coupled oscillator model. The Hamiltonian of the system is given by

$$\mathcal{H} = \begin{pmatrix} E_m - i\gamma_m & g \\ g & E_s - i\gamma_s \end{pmatrix}, \quad (2)$$

where the off-diagonal term g is the coupling strength, E_m and E_s are the energies of the molecular C=O bond and of the SLR, respectively, and γ_m and γ_s are the decoherence terms given by the linewidths of the molecular resonance and of the SLR, respectively. The values E_m and γ_m are obtained by fitting the measured C=O bond peak with a Voigt profile, while E_s and γ_s are obtained by fitting the extinction of the bare array with a period of $4 \mu\text{m}$ simulated with FDTD to a Fano line shape [20],

$$\sigma_F = \frac{(\varepsilon + q)^2}{\varepsilon^2 + 1}, \quad (3)$$

where q is the Fano parameter, $\varepsilon = \frac{E-E_0}{\gamma}$ is the reduced energy, and E_0 and γ are the energy and the width of the resonance, respectively. The fit to the simulation is shown in the SM, Sec. S4, also for different periods [43].

The eigenvalues associated to the Hamiltonian of Eq. (2) are calculated by solving the determinant $\det[\mathcal{H} - \lambda\hat{I}] = 0$, where λ are the eigenvalues and \hat{I} is the identity matrix (see SM, Sec. S5) [43]. The calculated eigenvalues are complex: the real components represent the energies of the lower and upper polaritons, while the imaginary components define the decoherence. From the energy difference between the lower and upper polaritons, we obtain a coupling constant $g = 40 \text{ cm}^{-1}$. We compare the modeled polariton energies and linewidths with the measured ones by fitting them to Eq. (3) (see SM, Sec. S6) [43]. Finally, we calculate the eigenvectors associated to Eq. (2). The coefficients of these eigenvectors are the Hopfield coefficients and their square represents the molecular or photonic fraction of the polaritons [45].

Figure 3(a) illustrates the comparison between the modeled (solid curve) and measured (circles) upper (red) and lower (black) polariton energies as a function of the SLR detuning from the C=O stretching of PMMA. We find that the model and measurements are in good agreement. The anticrossing behavior is typical of strongly coupled systems and shows the minimum splitting for the array with period of $\sim 4 \mu\text{m}$. In Fig. 3(b), we plot the full width at half maximum (FWHM) of the lower and upper polaritons. In general, we find that the measured linewidths of the polaritons follow the

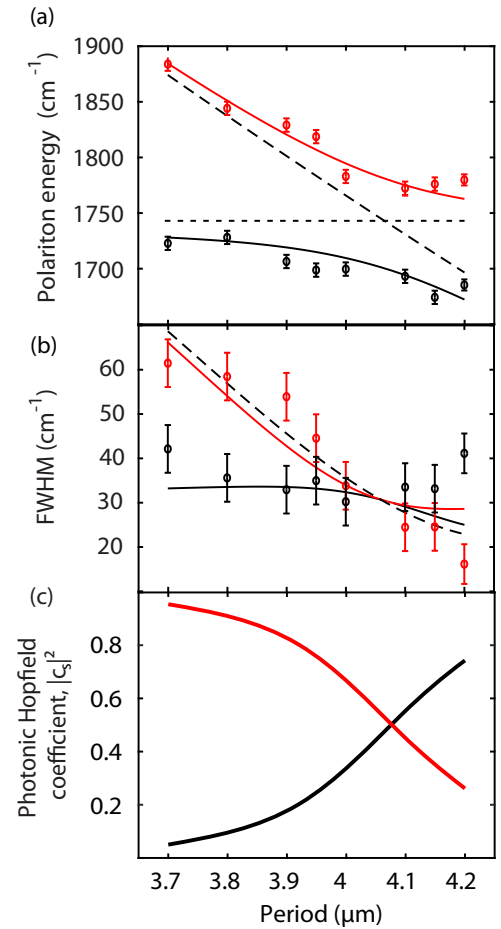


FIG. 3. (a) Lower (black) and upper (red) polariton energies as a function of the period of the array. The circles are the measurements. The solid curves are the modeled energies using a coupled oscillator model. The dashed and dotted lines represent the energies of the SLRs and of the C=O bond, respectively. (b) Lower (black) and upper (red) polariton linewidths as a function of the period of the microparticle arrays. The circles are the measurements and the solid curves are the modeled linewidths using a coupled oscillator model. The dotted curve represents the simulated linewidth of the SLRs. (c) Calculated Hopfield photonic mixing coefficient for the lower (black) and upper (black) polariton as a function of the period of the array.

behavior of the modeled polariton linewidths (solid curves). However, a consistent broadening of the measured lower polariton is found for array periods greater and smaller than $4 \mu\text{m}$ compared to the modeled linewidths. The unexpected but consistent behavior of the lower polariton linewidth for arrays with periods $3.7 \mu\text{m}$, $4.15 \mu\text{m}$, and $4.2 \mu\text{m}$ is not thus described by the coupled oscillator model and highlights the need for a more sophisticated model. Finally, we show, in Fig. 3(c), the photonic Hopfield coefficients for the lower and upper polaritons as a function of the period of the arrays, which corresponds to different cavity mode detunings from the C=O bond of PMMA. As expected, at smaller periods or larger SLR-PMMA detuning, the upper polariton has a more photonic behavior, while the lower polariton is mostly molecular.

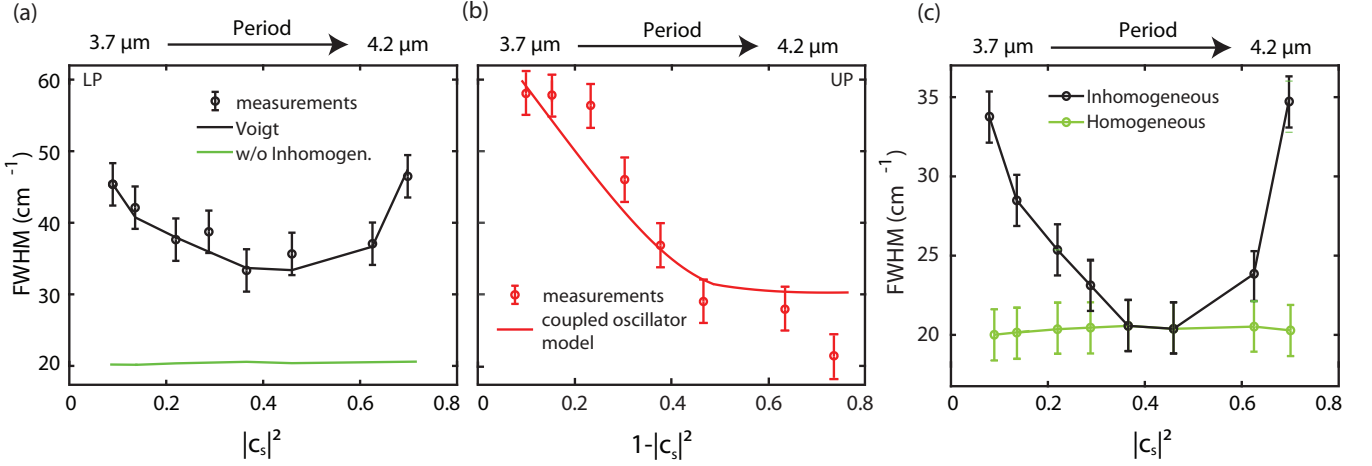


FIG. 4. Homogeneous and inhomogeneous broadening contribution to the linewidth of the lower and upper polaritons. (a) Measured (black circles) FWHM of the lower polariton as a function of the photonic mixing coefficient. The solid black curve is the polariton FWHM calculated with the inhomogeneous broadening contribution (Voigt profile). The green solid line is the polariton linewidth without inhomogeneous broadening. (b) Upper polariton experimental FWHM (circles) as a function of one-photonic mixing coefficient, to ease the comparison with the lower polariton case. The solid curve is the modeled FWHM with the coupled oscillator model. (c) Homogeneous (green) and inhomogeneous (black) contribution to the lower polariton linewidth. The solid curves are guides to the eye.

B. Vibropolaritons' motional narrowing

In general, there are two major contributions to the linewidth of a resonance: the homogeneous and the inhomogeneous broadening. For molecular vibrations, the homogeneous broadening is given by the intrinsic lifetime of the resonance, while the inhomogeneous broadening has two causes: (i) dephasing when single molecules experience different local environments, leading to slightly different vibrational frequencies, and (ii) the energy exchange between two identical molecules [46,47]. SLRs also experience a similar phenomenon, with an inhomogeneous broadening mainly caused by the nonuniform excitation of the SLR due to a noncollimated light source or with low spatial coherence, or by fabrication defects. Since polaritons are hybrid states, they possess the properties of molecular vibrations and photons. Thus, their linewidths suffer from the same inhomogeneous broadening as their molecular and photonic components. We experimentally reduce the SLR broadening by using the collimated beam of the FEL source with high spatial coherence. To explain the discrepancy between the measured linewidths of the lower polariton and the linewidths calculated with the coupled oscillator model, we show, in Fig. 4(a), the full width at half maximum of the lower polariton as a function of the photonic Hopfield coefficient $|c_s|^2$. The experimental linewidth of the lower polariton undergoes a reduction when the spectral overlap occurs between the surface lattice resonance (SLR) of the array and the C=O bond of PMMA. The linewidth reaches a minimum value when $|c_s|^2 \simeq 0.5$, where the lower polariton assumes a hybrid state with equal contributions from both its photonic and molecular components. For $|c_s|^2$ values larger or smaller than 0.5, the linewidth increases and the nature of the polariton is dominated either by its photonic or molecular component. First, we investigate the narrowing of the lower polariton by taking into consideration only the homogeneous broadening as [14]

$$\Delta f_p = (1 - |c_s|^2)\Delta f_m + |c_s|^2\Delta f_s, \quad (4)$$

where $\Delta f_{m,s}$ are the linewidths of the molecular (m) or photonic (s) resonance. The homogeneous linewidth of the lower polariton calculated with Eq. (4) is shown in Fig. 4(a) (green curve). We obtain Δf_s by simulating the SLRs for arrays with different periods. These simulations allow us to obtain a resonance without inhomogeneous broadening by considering an ideal system with infinite size, without imperfections, and illuminated by a collimated and coherent beam. Δf_m is extracted by fitting the carbonyl peak of PMMA with a Voigt profile (see SM, Sec. S7) [43] and considering only the Lorentzian contribution. Figure 4(a) clearly demonstrates that the behavior of the lower polariton linewidth cannot be solely explained by considering homogeneous broadening alone, as it deviates significantly from the experimental data. Thus, it can be concluded that the linewidth and narrowing of the lower polariton linewidth for $|c_s|^2 \sim 0.5$ is strongly influenced by inhomogeneous broadening.

To estimate the contribution of the inhomogeneous broadening to the lower polariton linewidth, we fit the FWHM of the lower polariton with the Voigt profile linewidth formula,

$$\Delta f_p = c_1\Delta f_p^H + \sqrt{c_2(\Delta f_p^H)^2 + c_3(\Delta f_p^{IH})^2}, \quad (5)$$

where $c_1 = 0.53$, $c_2 = 0.22$, and $c_3 = 1$ are empirical constants, calculated in Ref. [48], and Δf_p^H and Δf_p^{IH} are the homogeneous and inhomogeneous contribution to the polariton linewidth, respectively, with the latter chosen as the fitting parameter. The fit of the FWHM of the lower polariton to Eq. (5) is visible as a black solid curve in Fig. 4(a). In Eq. (5), the homogeneous contribution to the lower polariton linewidth is calculated from the theoretical coherence time (τ_p^H). Since the SLR and the carbonyl peak are in the strong coupling regime, the lower polariton coherence time is written as a combination of the molecular (τ_m) and photonic (τ_s)

homogeneous coherence times [14,49],

$$\tau_p^H = \frac{1}{\pi \Delta f_p^H} = \left(\frac{|c_s|^2}{\tau_s^H} + \frac{1 - |c_s|^2}{\tau_m^H} \right)^{-1}, \quad (6)$$

where [50]

$$\tau_m^H = \frac{1}{\pi \Delta f_m}, \quad \tau_s^H = \frac{1}{\pi \Delta f_s}. \quad (7)$$

We also show, in Fig. 4(b), the upper polariton linewidth as a function of $1 - |c_s|^2$. A constant broadening is observed, as the photonic mixing coefficient increases or $1 - |c_s|^2$ decreases. This behavior is consistent with previous studies on semiconductor microcavities [5,6], and it is well described by the coupled oscillators model [solid line in Fig. 4(b)].

In Fig. 4(c), we show the inhomogeneous and homogeneous contributions to the lower polariton linewidth plotted as function of the photonic mixing coefficient. We notice that the broadening of the lower polariton linewidths for Hopfield coefficients greater and smaller than 0.5 is caused by an increase of the inhomogeneous contribution. On the other hand, the homogeneous contribution to the lower polariton FWHM remains constant. Interestingly, we notice that for mixing coefficients close to 0.5, the inhomogeneous broadening is equal to the homogeneous contribution. The narrowing of the lower polariton observed in this study is consistent with previous works in the literature [1,5,6]. These studies demonstrate the existence of motional narrowing in exciton polaritons inside semiconductor Fabry-Perot cavities. Furthermore, they quantified this phenomenon by manipulating the temperature, transitioning from cryogenic to room temperature, thereby modulating the disorder within the system.

Our research reveals that vibropolaritons exhibit motional narrowing when studied at room temperature in open cavities created by resonant metasurfaces. The underlying cause of motional narrowing in vibropolaritons can be attributed to the delocalization of these polaritons on the surface of the plasmonic array. The presence of motional narrowing in vibropolaritons sustained by plasmonic particle arrays opens up

exciting avenues and tools to investigate polaritonic chemistry, where the collective behavior of coupled molecules exerts significant impact over chemical reactions [19,51–55].

IV. CONCLUSIONS

We have demonstrated experimentally vibrational strong coupling between SLRs in arrays of plasmonic microparticles and the C=O bond of PMMA using a free-electron laser as the infrared light source. We model the gold array/PMMA system with a coupled oscillator model to show that there is vibrational strong coupling. While this model succeeds in fitting the polariton energy, it fits poorly with the linewidth changes of the lower polariton for large detuning of the arrays' SLRs. We investigate these linewidth changes by calculating the inhomogeneous broadening contribution to the lower polariton linewidth. We notice that the inhomogeneous broadening becomes equal to the homogeneous broadening when the polariton mixing coefficients are close or equal to 0.5, while it broadens for large and small mixing coefficients. The strong dependence of the inhomogeneous narrowing of the lower polariton with the period of the array, which defines the coupling to the molecular vibration, suggests that this effect could be attributed to motional narrowing and the delocalization of the vibropolaritons on the surface of the microparticle array. Our investigation of motional narrowing of vibropolaritons offers insights into the strong coupling of molecular vibrations.

ACKNOWLEDGMENTS

F.V., J.G.R., and A.B. acknowledge Nils Dessmann for his assistance during the experiments, and Mohammad Ramezani for the fruitful discussions. J.G.R. acknowledges financial support from the Dutch Research Council (NWO) through the talent scheme (Vici Grant No. 680-47-628). A.B. acknowledges support from the Dutch Research Council (NWO) through the talent scheme (Vidi Grant No. 680-47-550).

-
- [1] V. Savona, C. Piermarocchi, A. Quattropani, F. Tassone, and P. Schwendimann, Microscopic theory of motional narrowing of microcavity polaritons in a disordered potential, *Phys. Rev. Lett.* **78**, 4470 (1997).
- [2] R. Tam and A. May, Motional narrowing of the rotational Raman band of compressed CO, N₂, and CO₂, *Can. J. Phys.* **61**, 1558 (1983).
- [3] K. O. Douglass, B. C. Dian, G. G. Brown, J. E. Johns, P. M. Nair, and B. H. Pate, Motional narrowing of the rotational spectrum of trifluoropropyne at 6550 cm⁻¹ by intramolecular vibrational energy redistribution, *J. Chem. Phys.* **121**, 6845 (2004).
- [4] J. D. Smith, R. J. Saykally, and P. L. Geissler, The effects of dissolved Halide anions on hydrogen bonding in liquid water, *J. Am. Chem. Soc.* **129**, 13847 (2007).
- [5] D.M. Whittaker, P. Kinsler, T. A. Fisher, M. S. Skolnick, A. Armitage, A. M. Afshar, M. D. Sturge, J. S. Roberts, G. Hill, and M. A. Pate, Motional narrowing in semiconductor microcavities, *Phys. Rev. Lett.* **77**, 4792 (1996).
- [6] D. M. Whittaker, What determines inhomogeneous linewidths in semiconductor microcavities?, *Phys. Rev. Lett.* **80**, 4791 (1998).
- [7] P. Borri, W. Langbein, U. Woggon, J. R. Jensen, and J. M. Hvam, Microcavity polariton linewidths in the weak-disorder regime, *Phys. Rev. B* **63**, 035307 (2000).
- [8] P. Borri, J. R. Jensen, W. Langbein, and J. M. Hvam, Direct evidence of reduced dynamic scattering in the lower polariton of a semiconductor microcavity, *Phys. Rev. B* **61**, R13377 (2000).
- [9] A. V. Kavokin and J. J. Baumberg, Exciton-light coupling in quantum wells: From motional narrowing to superradiance, *Phys. Rev. B* **57**, R12697 (1998).
- [10] J.J. Baumberg, A. P. Heberle, A. V. Kavokin, M. R. Vladimirova, and K. Köhler, Polariton motional narrowing in semiconductor multiple quantum wells, *Phys. Rev. Lett.* **80**, 3567 (1998).
- [11] P. Lukan, D. Sarchi, and V. Savona, Theory of trapped polaritons in patterned microcavities, *Phys. Stat. Sol. C* **3**, 2428 (2006).

- [12] A. Berthelot, I. Favero, G. Cassabois, C. Voisin, C. Delalande, P. Roussignol, R. Ferreira, and J.-M. Gérard, Unconventional motional narrowing in the optical spectrum of a semiconductor quantum dot, *Nat. Phys.* **2**, 759 (2006).
- [13] A. Laucht, N. Hauke, J.M. Villas-Bôas, F. Hofbauer, G. Böhm, M. Kaniber, and J.J. Finley, Dephasing of exciton polaritons in photoexcited ingaas quantum dots in GaAs nanocavities, *Phys. Rev. Lett.* **103**, 087405 (2009).
- [14] M. Wurdack, E. Estrecho, S. Todd, T. Yun, M. Pieczarka, S. Earl, J. Davis, C. Schneider, A. Truscott, and E. Ostrovskaya, Motional narrowing, ballistic transport, and trapping of room-temperature exciton polaritons in an atomically-thin semiconductor, *Nat. Commun.* **12**, 5366 (2021).
- [15] M. Skolnick, T. Fisher, and D. Whittaker, Strong coupling phenomena in quantum microcavity structures, *Semicond. Sci. Technol.* **13**, 645 (1998).
- [16] R. Houdré, Early stages of continuous wave experiments on cavity-polaritons, *Phys. Stat. Sol. (B)* **242**, 2167 (2005).
- [17] P. Törmä and W. L. Barnes, Strong coupling between surface plasmon polaritons and emitters: A review, *Rep. Prog. Phys.* **78**, 013901 (2014).
- [18] T. W. Ebbesen, Hybrid light-matter states in a molecular and material science perspective, *Acc. Chem. Res.* **49**, 2403 (2016).
- [19] K. Nagarajan, A. Thomas, and T. W. Ebbesen, Chemistry under vibrational strong coupling, *J. Am. Chem. Soc.* **143**, 16877 (2021).
- [20] S. R. K. Rodriguez, A. Abass, B. Maes, O. T. A. Janssen, G. Vecchi, and J. Gomez Rivas, Coupling bright and dark plasmonic lattice resonances, *Phys. Rev. X* **1**, 021019 (2011).
- [21] V. G. Kravets, A. V. Kabashin, W. L. Barnes, and A. N. Grigorenko, Plasmonic surface lattice resonances: A review of properties and applications, *Chem. Rev.* **118**, 5912 (2018).
- [22] W. Wang, M. Ramezani, A. I. Väkeväinen, P. Törmä, J. Gomez Rivas, and T. W. Odom, The rich photonic world of plasmonic nanoparticle arrays, *Mater. Today* **21**, 303 (2018).
- [23] C. Cherqui, M. R. Bourgeois, D. Wang, and G. C. Schatz, Plasmonic surface lattice resonances: Theory and computation, *Acc. Chem. Res.* **52**, 2548 (2019).
- [24] A. D. Utyushev, V. I. Zakomirnyi, and I. L. Rasskazov, Collective lattice resonances: Plasmonics and beyond, *Rev. Phys.* **6**, 100051 (2021).
- [25] G. Vecchi, V. Giannini, and J. Gomez Rivas, Shaping the fluorescent emission by lattice resonances in plasmonic crystals of nanoantennas, *Phys. Rev. Lett.* **102**, 146807 (2009).
- [26] A. G. Nikitin, A. V. Kabashin, and H. Dallaporta, Plasmonic resonances in diffractive arrays of gold nanoantennas: Near and far field effects, *Opt. Express* **20**, 27941 (2012).
- [27] A. Thomas, L. Lethuillier-Karl, K. Nagarajan, R. M. Vergauwe, J. George, T. Chervy, A. Shalabney, E. Devaux, C. Genet, J. Moran *et al.*, Tilting a ground-state reactivity landscape by vibrational strong coupling, *Science* **363**, 615 (2019).
- [28] K. Hirai, J. A. Hutchison, and H. Uji-i, Recent progress in vibropolaritonic chemistry, *ChemPlusChem* **85**, 1981 (2020).
- [29] P. Offermans, M. C. Schaafsma, S. R. Rodriguez, Y. Zhang, M. Crego-Calama, S. H. Brongersma, and J. Gómez Rivas, Universal scaling of the figure of merit of plasmonic sensors, *ACS Nano* **5**, 5151 (2011).
- [30] K.-H. Chang, J.-S. Cheng, T.-W. Lu, and P.-T. Lee, Engineering surface lattice resonance of elliptical gold nanodisk array for enhanced strain sensing, *Opt. Express* **26**, 33215 (2018).
- [31] A. Danilov, G. Tselikov, F. Wu, V. G. Kravets, I. Ozerov, F. Bedu, A. N. Grigorenko, and A. V. Kabashin, Ultranarrow surface lattice resonances in plasmonic metamaterial arrays for biosensing applications, *Biosens. Bioelectron.* **104**, 102 (2018).
- [32] F. A. A. Nugroho, P. Bai, I. Darmadi, G. W. Castellanos, J. Fritzsche, C. Langhammer, J. G. Rivas, and A. Baldi, Inverse designed plasmonic metasurface with parts per billion optical hydrogen detection, *Nat. Commun.* **13**, 5737 (2022).
- [33] L. Wang, Q. Wang, T.-Q. Wang, W.-M. Zhao, X.-Y. Yin, J.-X. Jiang, and S.-S. Zhang, Plasmonic crescent nanoarray-based surface lattice resonance sensor with a high figure of merit, *Nanoscale* **14**, 6144 (2022).
- [34] R. Adato, A. A. Yanik, J. J. Amsden, D. L. Kaplan, F. G. Omenetto, M. K. Hong, S. Erramilli, and H. Altug, Ultra-sensitive vibrational spectroscopy of protein monolayers with plasmonic nanoantenna arrays, *Proc. Natl. Acad. Sci. USA* **106**, 19227 (2009).
- [35] A. A. Yanik, A. E. Cetin, M. Huang, A. Artar, S. H. Mousavi, A. Khanikaev, J. H. Connor, G. Shvets, and H. Altug, Seeing protein monolayers with naked eye through plasmonic fano resonances, *Proc. Natl. Acad. Sci. USA* **108**, 11784 (2011).
- [36] R. La Rocca, G. C. Messina, M. Dipalo, V. Shalabaeva, and F. De Angelis, Out-of-plane plasmonic antennas for Raman analysis in living cells, *Small* **11**, 4632 (2015).
- [37] S. Zhang, N. Nishi, and T. Sakka, Electrochemical surface plasmon resonance measurements of camel-shaped static capacitance and slow dynamics of electric double layer structure at the ionic liquid/electrode interface, *J. Chem. Phys.* **153**, 044707 (2020).
- [38] K. Murakoshi, H. Minamimoto, and T. Hayashi, Electrochemical control of dye molecule excitation strongly coupled with plasmonic surface lattice resonance, in *ECS Meeting Abstracts*, Vol. 15 (IOP, Bristol, UK, 2021), p. 711.
- [39] B. Cohn, K. Das, A. Basu, and L. Chuntonov, Infrared open cavities for strong vibrational coupling, *J. Phys. Chem. Lett.* **12**, 7060 (2021).
- [40] F. Verdelli, J. J. Schulpen, A. Baldi, and J. G. Rivas, Chasing vibro-polariton fingerprints in infrared and raman spectra using surface lattice resonances on extended metasurfaces, *J. Phys. Chem. C* **126**, 7143 (2022).
- [41] H. Li, Refractive index of alkaline earth halides and its wavelength and temperature derivatives, *J. Phys. Chem. Ref. Data* **9**, 161 (1980).
- [42] E. D. Palik, *Handbook of Optical Constants of Solids*, Vol. 3 (Academic, Boston, MA, 1998).
- [43] See Supplemental Material at <http://link.aps.org/supplemental/10.1103/PhysRevB.109.174305> for additional information regarding sample preparation and characterization, additional data, and theoretical models.
- [44] S. Tsuda, S. Yamaguchi, Y. Kanamori, and H. Yugami, Spectral and angular shaping of infrared radiation in a polymer resonator with molecular vibrational modes, *Opt. Express* **26**, 6899 (2018).
- [45] J. Hopfield, Theory of the contribution of excitons to the complex dielectric constant of crystals, *Phys. Rev.* **112**, 1555 (1958).
- [46] R. J. Abbott and D. W. Oxtoby, Exchange dephasing and motional narrowing of vibrational modes, *J. Chem. Phys.* **70**, 4703 (1979).
- [47] E. Knapp, Lineshapes of molecular aggregates, exchange narrowing and intersite correlation, *Chem. Phys.* **85**, 73 (1984).

- [48] J. J. Olivero and R. Longbothum, Empirical fits to the Voigt line width: A brief review, *J. Quantum Spectrosc. Radiat. Transfer* **17**, 233 (1977).
- [49] H. Deng, H. Haug, and Y. Yamamoto, Exciton-polariton Bose-Einstein condensation, *Rev. Mod. Phys.* **82**, 1489 (2010).
- [50] M. E. Reimer, G. Bulgarini, A. Fognini, R. W. Heeres, B. J. Witek, M. A. M. Versteegh, A. Rubino, T. Braun, M. Kamp, S. Höfling, D. Dalacu, J. Lapointe, P. J. Poole, and V. Zwiller, Overcoming power broadening of the quantum dot emission in a pure wurtzite nanowire, *Phys. Rev. B* **93**, 195316 (2016).
- [51] M. A. Zeb, P. G. Kirton, and J. Keeling, Exact states and spectra of vibrationally dressed polaritons, *ACS Photon.* **5**, 249 (2018).
- [52] R. F. Ribeiro, L. A. Martínez-Martínez, M. Du, J. Campos-Gonzalez-Angulo, and J. Yuen-Zhou, Polariton chemistry: Controlling molecular dynamics with optical cavities, *Chem. Sci.* **9**, 6325 (2018).
- [53] J. Feist, J. Galego, and F. J. Garcia-Vidal, Polaritonic chemistry with organic molecules, *ACS Photon.* **5**, 205 (2018).
- [54] F. Herrera and J. Owrutsky, Molecular polaritons for controlling chemistry with quantum optics, *J. Chem. Phys.* **152**, 100902 (2020).
- [55] F. J. Garcia-Vidal, C. Ciuti, and T. W. Ebbesen, Manipulating matter by strong coupling to vacuum fields, *Science* **373**, eabd0336 (2021).